Volumetric recombination in EMC3-EIRENE: implementation, and first application to the pre-fusion power operation phase in ITER

H. Frerichs,[1,*] Y. Feng,[2] X. Bonnin,[3] R.A. Pitts,[3] D. Reiter,[4] and O. Schmitz[1]

[1] *University of Wisconsin - Madison, Department of Engineering Physics, Madison, Wisconsin, 53706, USA*
[2] *Max-Planck-Institut für Plasmaphysik, Association EURATOM-IPP, 17491 Greifswald, Germany*
[3] *ITER Organization, Route de Vinon-sur-Verdon, CS 90 046, 13067 St Paul Lez Durance Cedex, France*
[4] *Institute for Laser and Plasma Physics, Heinrich-Heine-University, D-40225 Duesseldorf, Germany*

(Dated: September 8, 2021)

An upgrade to the 3-D plasma boundary model EMC3-EIRENE for detached divertor plasmas is introduced and evaluated. Stabilization of the iterative approximation of a self-consistent plasma - neutral gas solution is required at low divertor plasma temperatures, and this has been achieved by linearization of the energy loss term associated with electron - neutral gas interaction. An implicit method for volumetric recombination has been implemented, which improves agreement with SOLPS-ITER results for the pre-fusion power operation phase in ITER. Resonant magnetic perturbations for control of edge localized modes are found to result in a partially detached divertor plasma with a significantly broader reduction of particle loads in the traditional strike zone, which is attributed to volumetric recombination. The additional non axisymmetric far scrape-off layer strike points, on the other hand, remain attached at relatively high temperature so that volumetric recombination is not effective there.

I. INTRODUCTION

Numerical models play a pivotal role in designing new magnetic fusion experiments, and designing the ITER divertor for efficient pumping and density control without extreme heat loads is one particular application [1]. In particular, the design of the first ITER tungsten divertor [2] is based on extensive 2-D modeling of the plasma boundary with the SOLPS-4.3 and SOLPS-ITER codes [3, 4], which exploit the traditional assumption of toroidal symmetry in tokamaks. However, standard high confinement (H-mode) operation implies edge localized modes (ELMs) - a quasi-periodic MHD instability in the plasma edge - which need to be controlled (suppressed or significantly mitigated) in ITER because of the potential damage to plasma-facing components (divertor targets/plates). The leading method for ELM control today is the application of resonant magnetic perturbations (RMPs), a method pioneered at the DIII-D tokamak [5] and successfully reproduced in many other experiments. But while a dedicated set of ELM control coils has been integrated into the ITER device [6], symmetry breaking effects from RMP application cannot be accounted for in 2-D models of the plasma boundary, and their implications for a partially detached divertor plasma with reduced heat loads remain to be evaluated.

The EMC3 fluid plasma model [7, 8] (coupled to EIRENE [9, 10] for interaction with neutral particles) has been initially developed for the intrinsically 3-D plasma boundary in stellarators, but its flexible geometry representation readily allows application to tokamaks with RMPs [11]. On the physics side, however, development of EMC3 is still behind its 2-D counterparts (for example the B2 and B2.5 fluid plasma codes in the SOLPS-4.3 and SOLPS-ITER packages respectively). In particular, volumetric recombination - a process that becomes relevant in the divertor once the temperature drops to a few eV - has not been included so far. Furthermore, it appears that modeling of plasma detachment in poloidal divertor tokamaks is more challenging than in stellarators [12] (perhaps because of the longer field line connection lengths in the latter which result in a relatively higher importance of cross-field transport effects over neutral gas interactions). Numerical oscillations of divertor plasma temperature and density appear, and a self-consistent solution cannot be reached. Despite promising first results from adaptive relaxation [13], robust stabilization has not been achieved. Rather than healing the symptoms, a new approach based on the linearization of energy losses has been developed recently [14] which may be more closely linked to the source of this numerical instability.

In this paper, we introduce and evaluate an upgrade of EMC3-EIRENE for numerical access to detached divertor plasmas. First, the EMC3-EIRENE model is presented in section II with a review of stabilization at low temperatures in section II A. Implementation of volumetric recombination is then described in section II B. Finally, convergence and particle balance control is addressed in section II C. Following the "staged approach" of the ITER Research Plan [15], we take the first step of evaluating the upgraded EMC3-EIRENE for the first Pre-Fusion Power Operation phase (PFPO-I). After comparing results for the toroidally symmetric equilibrium with results from SOLPS-ITER, we evaluate RMP effects on divertor detachment in section III for one particular case.

* hfrerichs@wisc.edu

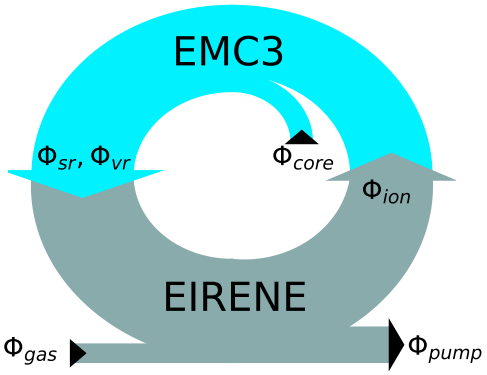

FIG. 1. Overall particle balance in the coupled plasma (EMC3) and neutral gas (EIRENE) system. External sources from gas fueling ($\Phi_{\rm gas}$) and core fueling ($\Phi_{\rm core}$) are balanced by pumping ($\Phi_{\rm pump}$). Surface (Φ_{sr}) and volume recombination (Φ_{vr}) are sources for the neutral gas, and (re-)ionization ($\Phi_{\rm ion}$) sustains the plasma.

II. THE EMC3-EIRENE MODEL

The EMC3 model follows the SOLPS approach in that the plasma is described by a fluid model, and differs only in that a steady state solution is obtained by iterative approximation in EMC3 rather than by following a time derivative. This requires that external fueling from gas puffing ($\Phi_{\rm gas}$), and pellets and neutral beam injection into the core ($\Phi_{\rm core}$) is balanced by pumping (i.e. global particle balance, figure 1):

$$\underbrace{\Phi_{\rm fuel}}_{=\Phi_{\rm gas}+\Phi_{\rm core}} = \Phi_{\rm pump}. \qquad (1)$$

A self-consistent solution requires iterative application of EMC3 for the boundary plasma and EIRENE for the neutral gas. Specifically, the plasma density n_i is determined by the local particle balance

$$\nabla\cdot\left[n_i u_\parallel \mathbf{e}_\parallel - D_\perp \mathbf{e}_\perp\mathbf{e}_\perp\cdot\nabla n_i\right] = S_p \qquad (2)$$

where $u_\parallel$ is the plasma flow velocity along magnetic field lines. Here, $\mathbf{e}_\parallel = \mathbf{B}/|\mathbf{B}|$ is the unit vector in direction of the magnetic field and $\mathbf{e}_\perp\mathbf{e}_\perp = 1 - \mathbf{e}_\parallel\mathbf{e}_\parallel$ is the dyadic product for the cross-field direction. Anomalous cross-field transport is taken into account by a free model parameter $D_\perp$. The right hand side of (2) includes sources from ionization of atoms and dissociative ionization channels of molecules as computed by EIRENE, and - following section II B - sinks from volumetric recombination (see table I in [16] for list of processes included in the present simulations). Quasi-neutrality is assumed in EMC3, which implies $n_e = n_i$ for the main (hydrogen) ion species.

The plasma flow velocity $u_\parallel$ in (2) is determined by momentum balance along field lines

$$\nabla\cdot\left[m_i n_i u_\parallel^2\mathbf{e}_\parallel - \eta_\parallel\mathbf{e}_\parallel\mathbf{e}_\parallel\cdot\nabla u_\parallel - D_\perp\mathbf{e}_\perp\mathbf{e}_\perp\cdot\nabla\left(m_i n_i u_\parallel\right)\right] = -\mathbf{e}_\parallel\cdot\nabla\left(p_e+p_i\right) + S_m \qquad (3)$$

which includes the electron pressure gradient on the right hand side (RHS) following an approximation for the electric field along the field line direction. Cross-field viscosity is implicitly set to $\eta_\perp = m_i\, n_i\, D_\perp$ and viscosity from transport along field lines $\eta_\parallel$ is classical. Momentum loss (or gain) from charge exchange between ions and neutral particles is included in S_m, as well as momentum exchange from the volumetric recombination processes. Temperatures T_e and T_i are separated between electrons and ions, and are determined by the local energy balances

$$\nabla\cdot\left[\tfrac{5}{2}T_e n_i u_\parallel\mathbf{e}_\parallel - \kappa_e\mathbf{e}_\parallel\mathbf{e}_\parallel\cdot\nabla T_e - \tfrac{5}{2}T_e D_\perp\mathbf{e}_\perp\mathbf{e}_\perp\cdot\nabla n_i - \chi_e n_i\,\mathbf{e}_\perp\mathbf{e}_\perp\cdot\nabla T_e\right] - k\left(T_i-T_e\right) = S_{ee} \qquad (4)$$

$$\nabla\cdot\left[\tfrac{5}{2}T_i n_i u_\parallel\mathbf{e}_\parallel - \kappa_e\mathbf{i}_\parallel\mathbf{e}_\parallel\cdot\nabla T_i - \tfrac{5}{2}T_i D_\perp\mathbf{e}_\perp\mathbf{e}_\perp\cdot\nabla n_i - \chi_i n_i\,\mathbf{e}_\perp\mathbf{e}_\perp\cdot\nabla T_i\right] + k\left(T_i-T_e\right) = S_{ei} \qquad (5)$$

which are coupled through the energy exchange term on the RHS with $k = 3\,m_e/m_i\cdot n_i/\tau_e$. Spitzer heat conductivity κ_e and κ_i is applied along field lines (presently without a flux limit in EMC3) while free model parameters χ_e and χ_i account for anomalous cross-field heat transport. Energy losses from interaction with neutral particles (excitation, ionization, molecular dissociation and charge exchange) are included in S_{ee} and S_{ei}. Even though a trace impurity model is available in EMC3 for cooling of electrons through S_{ee} due to impurity radiation [12], it is neglected here because impurity seeding is not anticipated in PFPO-1 (unlike for the burning plasma phase).

One particular challenge is the electron cooling term (S_{ee}) when it starts to play a significant role in the total power balance, because rate coefficients for the associated processes are very sensitive to small changes at low T_e (they vary by several orders of magnitude over a range of a few eV). Previously, simulations have been found to become unstable when T_e drops below $5-10\,$eV, or rather they appear to be attracted to a T_e-n_i cycle without convergence to a self consistent solution [12–14]. In fact, impurity radiation posed the same numerical problem, which was overcome by linearizing the impurity cooling rate [17]. However, the energy loss due to the hydrogen isotope neutral particles has only been linearized recently [14] after numerical instabilities emerged in tokamak applications under high density and low temperature conditions (in the absence of impurity radiation).

This behavior is demonstrated in figure 2 (a-d) where simulation results are characterized by average values $\overline{T}_e$ and $\overline{n}_i$ at the inner and outer targets. Simulation parameters in this section are set for an unperturbed configuration after particle flux roll-over is expected from SOLPS-ITER (IDS case 102298/3 in the IMAS ITER database): anomalous cross-field transport is $D_\perp = 0.3\,\mathrm{m^2\,s^{-1}}$ and $\chi_{e\perp} = \chi_{i\perp} = 1\,\mathrm{m^2\,s^{-1}}$, parallel viscosity $\eta_\parallel$ is neglected, gas fueling is $\Phi_{\mathrm{gas}} = 3.3 \cdot 10^{22}\,\mathrm{s^{-1}}$ with core fueling of $\Phi_{\mathrm{core}} = 6 \cdot 10^{20}\,\mathrm{s^{-1}}$ and pumping (sticking fraction) of $7.2 \cdot 10^{-3}$ on the sub-divertor floor. Power input into the simulation domain is $P_{\mathrm{SOL}} = 20\,\mathrm{MW}$.

A. Stabilization at low temperatures

The iterative approximation of a self-consistent solution between the plasma solver (EMC3) and the neutral gas solver (EIRENE) implies that the left hand side (LHS) of the energy balance (4) is solved for a given RHS (the EMC3 step), and that the RHS is calculated (the EIRENE step) based on a given temperature. While S_{ee} is fed back to the next iteration of solving the LHS of (4), its given value may be significantly different from what it would be if it had been calculated based on the new resulting T_e. The strong non-linearity of the underlying reactions may be responsible for the unstable behavior[18] observed in figure 2. A contributing factor appears to be the grid resolution: benchmarks for a 1-D flux tube showed that oscillations arise at low resolution in front of the target when changes in the temperature differential between cells trigger a substantial increase of radiation in one cell without a balanced decrease in the adjacent cell. In particular, it can be seen in figure 2 (a,e) that the divertor plasma oscillates between an attached state (light blue with $\overline{T}_e \approx 10\,\mathrm{eV}$) and a deeply detached one (dark blue with $\overline{T}_e \approx 1\,\mathrm{eV}$) at the inner target. The deeply detached state is apparent in figure 2 (e) where T_e stays below 1 eV up to 17 cm from the separatrix strike point, while the attached state has a peak T_e of 25 eV with significant particle and heat loads. Furthermore, it can be seen in figure 2 (b,f) that the divertor plasma at the outer target oscillates similarly, but with the opposite phase. The density may appear to counteract the temperature oscillations, but actually shows some form of hysteresis effect as discussed in a simplified model [13].

Stabilization of the iterative approximation can be achieved with a linearization of S_{ee} as has been recently highlighted [14], and in the following we will elaborate on those results. Following the same strategy as for the treatment of impurity radiation, a predictive representation of S_{ee} for the j-th iteration of (4) is based on a (locally evaluated) Taylor expansion at $T_e^{(j-1)}$

$$S_{ee}^{(j)} \approx S_{ee}\left(T_e^{(j-1)}\right) + \left(T_e^{(j)} - T_e^{(j-1)}\right) \left.\frac{dS_{ee}}{dT_e}\right|_{T_e^{(j-1)}} \tag{6}$$

where $T_e^{(j-1)}$ is known from the previous iteration. The first term on the RHS is part of the traditional coupling between EMC3 and EIRENE, while the second term allows for an approximation of S_{ee} that is consistent with $T_e^{(j)}$ at the end of this iteration (see appendix A for details on the implementation). One should note that this does not change the physics model (2)-(5) since the correction term vanishes once a self consistent solution has been reached.

The green traces in figure 2 (a-d) show the development of characteristic parameters once S_{ee} linearization is switched on. It can be seen that the plasma state stops oscillating within a couple iterations and then remains stable for at least 100 iterations. After 24 iterations, linear regression shows that only a weak change of 0.1 % and 2.3 % over the next 40 iterations is found for $\overline{T}_e$ at the inner and outer targets, respectively. Nevertheless, a slowly drifting result with a change of 7.2 % and −4.7 % is still found for $\overline{n}_i$ during this phase. Afterwards, both $\overline{T}_e$ and $\overline{n}_i$ are at or below 2 % for the next 96 iterations. While it is impractical to keep the 3-D simulation results from each iteration for averaging at a later point, an optional cumulative average has been implemented which is updated and stored along with (but not affecting) the simulation results. This cumulative average can be restarted at any point, if a slow transient is found in the results while monitoring the progress. The results in section III are based on a cumulative average over 128 iterations for noise reduction.

The T_e profiles in figure 2 (e-f) show that the resulting state is a partially detached one in between the two extreme states of attached and deeply detached which are seen during oscillations. Comparison with SOLPS-ITER results (black profiles) for the same model parameters (and similar resulting upstream density of $2 \cdot 10^{19}\,\mathrm{m^{-3}}$ at the outboard midplane) show good agreement, at least for the low T_e detachment zone next to the separatrix strike point (T_e in the far SOL tends to be lower in the EMC3-EIRENE simulations, but these values are less important because of the low particle and heat loads there). The density profiles in figure 2 (g-h) show that the peak density of $1.0 \cdot 10^{21}\,\mathrm{m^{-3}}$ at the inner target is located closer to the strike point and exceeds the value of $0.64 \cdot 10^{21}\,\mathrm{m^{-3}}$ found in the SOLPS-ITER simulation. The trend is similar on the outer target. The density profiles in the EMC3-EIRENE simulation are broader on the left side into the private flux region (PFR), but reproduce the ones in the SOLPS-ITER simulation well on the right side into the scrape-off layer (SOL) from a distance of 3 cm outwards (the location of the peak density in the SOLPS-ITER simulation).

B. Volumetric recombination

With stabilization at low divertor T_e, we can now turn to the implementation of volumetric electron-ion recombination (EIR, $e + D^+ \rightarrow D$) into EMC3-EIRENE. Con-

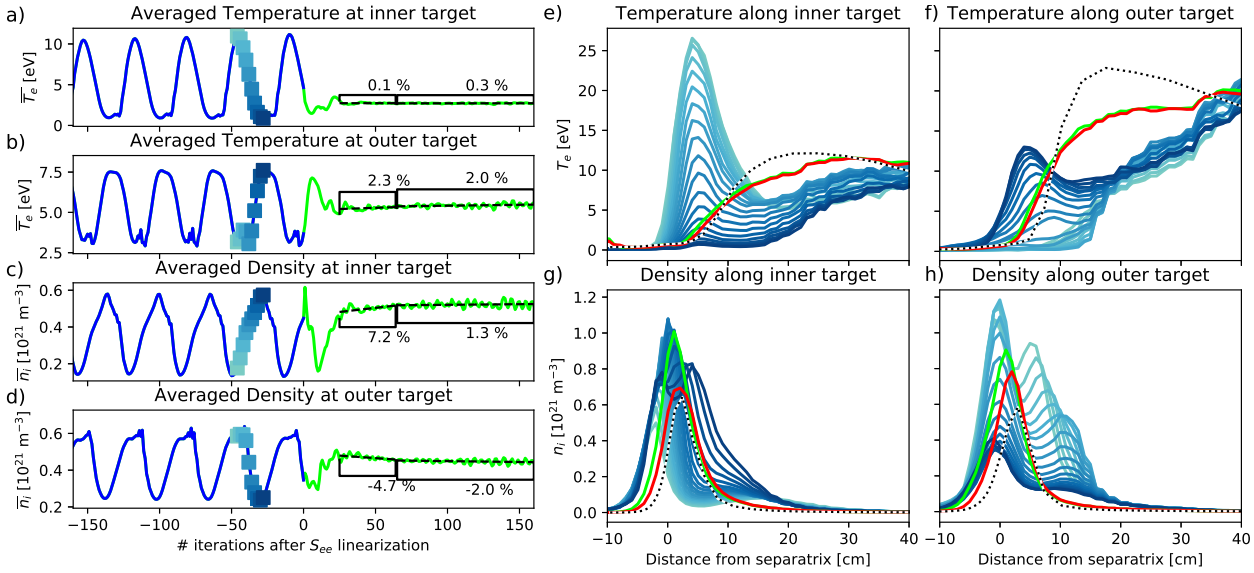

FIG. 2. (a-d) Simulation history of the pressure weighted average temperature $\overline{T}_e$ and density $\overline{n}_i$ at the inner and outer targets, respectively. (e-h) Profiles along the inner and outer targets during oscillations (shades of blue) as indicated by the coloured symbols in (a-d), converged results after S_{ee} linearization (green) and implementation of volume recombination (red), and results from SOLPS-ITER (black dotted).

tributions to the RHSs of (2)-(3) from EIR are:

$$S_{p\,vr} = -\,n_i\,n_e\,\langle\sigma_{vr}\,v\rangle \tag{7}$$

$$S_{m\,vr} = -\,m_i\,u_\parallel\,n_i\,n_e\,\langle\sigma_{vr}\,v\rangle \tag{8}$$

$$S_{ee\,vr} = E_i\,\langle\sigma_{vr}\,v\rangle\;-\;\text{H.10} \tag{9}$$

$$S_{ei\,vr} = -\left(\frac{1}{2}\,m_i\,u^2 + \frac{3}{2}\,T_i\right)\,n_i\,n_e\,\langle\sigma_{vr}\,v\rangle \tag{10}$$

where $\langle\sigma_{vr}\,v\rangle$ is the rate coefficient H.4 2.1.8 taken from the AMJUEL database[19], E_i is the ionization potential, and H.10 is the associated radiation loss coefficient that is to be applied in combination with $E_i\,\langle\sigma_{vr}\,v\rangle$ for the total electron cooling rate[20]. The kinetic energy term in (10) is neglected in the following, because the corresponding term is already neglected on the LFS of the model equation (5). Numerical solution of (2)-(5) in EMC3 is split into two steps: the two energy balances are solved in one step (ENERGY), and the particle and momentum balances are solved in another step (STREAMING). The latter step is based on the linear combinations

$$\frac{1}{2}\left[(2.\text{L}) \pm \frac{1}{m_i\,c_s}\,(3.\text{L})\right] = \frac{1}{2}\left[(2.\text{R}) \pm \frac{1}{m_i\,c_s}\,(3.\text{R})\right] \tag{11}$$

of the left hand right hand sides of (2) and (3). One can interpret the linear combinations (11) as balance equations for virtual fluid parcels traveling at sound speed c_s in forward (+) or backward (-) direction along a field line. Implementation of volumetric recombination requires evaluation of the corresponding sink term in (11). Plugging (7) and (8) into (11)'s RHS, we find

$$S_{\pm\,vr} = -\underbrace{\frac{n_i}{2}\,(1 \pm M)}_{=n_\pm}\,\underbrace{n_e\,\langle\sigma_{vr}\,v\rangle}_{=\mathcal{R}} \tag{12}$$

where $n_\pm$ are the dummy densities associated with the virtual fluid parcels. These are related to the plasma density and Mach number $M = u_\parallel/c_s$:

$$n_i = n_+ + n_- \qquad \text{and} \qquad M = \frac{n_+ - n_-}{n_+ + n_-}. \tag{13}$$

We consider the recombination rate per ion $\mathcal{R}$ as fixed during one iteration, and recognize the generic, linearized form of (12) and (10)

$$\mathcal{S}_{vr} = -\alpha\,\mathcal{F}, \qquad \alpha = \begin{cases} \mathcal{R}, & \mathcal{F} = n_\pm \\ \frac{3}{2}\,n_i\,\mathcal{R}, & \mathcal{F} = T_i \end{cases} \tag{14}$$

for application in the STREAMING and ENERGY steps (for the purpose of implementing (7)-(10), we consider $S_{ee\,vr}$ to be already included in S_{ee} in (4), because it is mostly a source term).

Even though the system (2)-(5) is steady state, a numerical time step τ is required for the Monte Carlo method that EMC3 is based upon[21]. A solution for (2)-(5) is approximated by sampling (and assigning weight to) Monte Carlo fluid parcels from a source distribution,

and steady state is implied by scoring their entire trajectory within a mesh until they reach a sink. The advantage of (14) is that it is naturally suited for an implicit, residual-free method: as $\mathcal{S}_{vr}$ represents the change of $\mathcal{F}$ with time, one can account for it in its linearized form simply by reducing the weight $w \rightarrow w \exp(-\alpha\,\tau)$ of the Monte Carlo parcels during each time step τ. I.e. the implicit method guarantees that the right amount of losses are accounted for, unlike in an explicit method which requires "enough" Monte Carlo parcels to reach a given sink. The same approach is suitable for the linearized energy sink from electron impact ionization and molecular dissociative ionization channels discussed above.

Profiles of T_e and n_i on the divertor targets are shown in figure 2 (e-h) from a simulation with volume recombination included (red). Here we find only a minor impact on T_e, but the peak n_i is reduced as expected from (plasma) particle losses due to recombination. While profiles from SOLPS (black) are not exactly reproduced, better agreement is found than for the simulation without volume recombination (green). Further validation is motivated by good agreement with experimental observations under detached conditions in small-ELM upper single null discharges at ASDEX-U [22] achieved with a preview version of the EMC3-EIRENE upgrade presented here.

C. Particle balance control

While gas puffing Φ_{gas} and core fueling Φ_{core} are fixed model parameters, the pumped flux Φ_{pump} is a result of the sticking fraction at the pump surface and the number of neutral particles that reach this surface. On the plasma side, particle sources from core fuelling and from ionization are balanced by recombination (see figure 1), either on the divertor target surfaces (Φ_{sr}) or in the divertor volume (Φ_{vr}):

$$\Phi_{\text{core}} + \Phi_{\text{ion}} = \Phi_{sr} + \Phi_{vr}. \tag{15}$$

Note that Φ_{ion} represents the entire ionization source including ionization of neutral particles in the core (which is taken into account in EMC3 by a corresponding plasma source on the core boundary of the EMC3 domain along with Φ_{core}). On the neutral gas side, particle sources from recombination and gas puffing are balanced by ionization and pumping:

$$\Phi_{sr} + \Phi_{vr} + \Phi_{\text{gas}} = \Phi_{\text{ion}} + \Phi_{\text{pump}}. \tag{16}$$

Depending on the control parameters selected in the simulation, equation (1) may not be fulfilled after an individual iteration of EMC3 or EIRENE. In order to reach a steady state, one can either a) leave the internal balances (15) and (16) untouched (i.e. stiff balance) and monitor the error

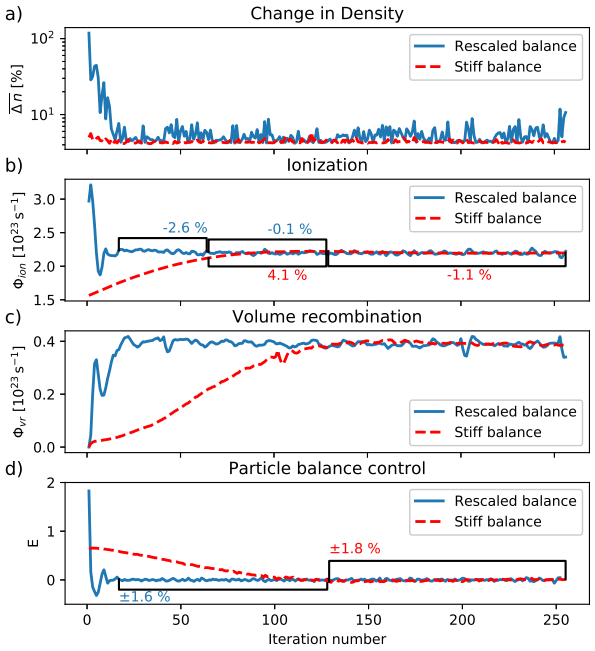

FIG. 3. (a-d) Simulation history of characteristic parameters for evaluation of convergence. A stiff particle balance (red) is compared to rescaling (blue) for convergence acceleration. The Simulation is started from a self-consistent solution for lower density and throughput.

$$E_{\text{stiff}} = \frac{\Phi_{\text{fuel}} - \Phi_{\text{pump}}}{\Phi_{\text{fuel}}} \tag{17}$$

over a number of iterations during which Φ_{ion} slowly builds up until it sustains the plasma in a way that the right amount of recycled neutral particles can be exhausted, or b) one can rescale Φ_{ion} after an EIRENE iteration so that (1) is implicitly fulfilled. More precisely, only the contributions from Φ_{sr} and Φ_{vr} to Φ_{ion} should be rescaled since the external sources Φ_{gas} remain fixed. The scaling factor

$$F = \frac{\Phi_{\text{ion}}(\Phi_{\text{gas}}) + \Phi_{\text{core}}}{\Phi_{\text{pump}}(\Phi_{sr}) + \Phi_{\text{pump}}(\Phi_{vr})} \tag{18}$$

is computed by tracking the individual contributions $\Phi_{\text{ion}}(S)$ and $\Phi_{\text{pump}}(S)$ from each source of neutral particles $S = \Phi_{sr}, \Phi_{vr}, \Phi_{\text{gas}}$. Convergence can be significantly accelerated if (18) is applied after each EIRENE step. This is demonstrated in figure 3 by comparing the two approaches for a simulation that has been initiated from a self-consistent solution at lower density and throughput (IDS case number 102297/3 in the IMAS ITER database). Figure 3 (a) shows the volume averaged relative change of the density $\overline{\Delta n}$ which is initially large for the rescaling approach but saturates at a level of 5 % (due to noise related to the Monte Carlo methods

in EMC3 and EIRENE) after only 16 iterations. Afterwards, a slow change of $-2.6\,\%$ over the next 48 iterations is still found for $\Phi_{\rm ion}$ in figure 3 (b), and this reduces to $-0.1\,\%$ for the next 64 iterations after that. The error

$$E_{\rm rescale} = F - 1 \tag{19}$$

for the rescaling approach remains within $\pm 1.6\,\%$ of a self-consistent particle balance after 16 iterations, as can be seen in figure 3 (d). For the stiff particle balance (red profiles), on the other hand, it can be seen that $\Phi_{\rm ion}$ and Φ_{vr} slowly build up over 128 iterations (resulting in an initially smaller $\overline{\Delta n}$). Eventually, the same $\Phi_{\rm ion}$ and Φ_{vr} is reached, and the error $E_{\rm stiff}$ remains within $\pm 1.8\,\%$ for the next 128 iterations at a similar level as $E_{\rm rescale}$. The stiff particle balance is clearly less efficient than the rescaled particle balance, but it can be seen in figure 3 (a) that it allows for a somewhat lower noise level $\overline{\Delta n}$. Even though the noise can be reduced by updating a cumulative average over iterations (or increasing the number of Monte Carlo particles used in each step), this may become useful if further stabilization is required.

III. RMP EFFECTS ON DIVERTOR DETACHMENT

We now exploit the extended application range of EMC3-EIRENE and evaluate RMP effects on divertor detachment (still for pre-fusion power operation, but at higher input power of $P_{\rm SOL} = 30\,$MW, accounting for an upgrade of an additional 10 MW ECRH heating which is currently under consideration). The RMP field including a linearized, resistive single fluid MHD plasma response, is provided by MARS-F [23]. RMPs are applied with toroidal mode number $n = 3$ at a phasing that has been optimized for ELM control based on maximizing the resulting X-point displacement as discussed in reference 24. The RMPs are produced with a current of 30 kAt ($= 5\,$kA $\cdot$ 6 turns) in the ELM control coils, i.e. the low field / low current equivalent of maximum strength available for the burning plasma phase. It should be noted that this does not take into account beneficial effects from optimizing the phase, which may result in lower required RMP currents for ELM suppression.

Initial results from a gas puff scan have been highlighted in reference 25, and we elaborate on these results here with a focus on the particle balance. First, we establish a foundation for comparing simulations with and without RMPs. While the upstream density is typically evaluated at the outboard midplane in axisymmetric tokamak configurations, this approach is not a suitable for RMP configurations. Because perturbed field lines can connect from the nominally confined plasma to the divertor targets guided by the helical oscillations of the perturbed separatrix, helical perturbations of the plasma density appear. This can be seen in the poloidal profiles

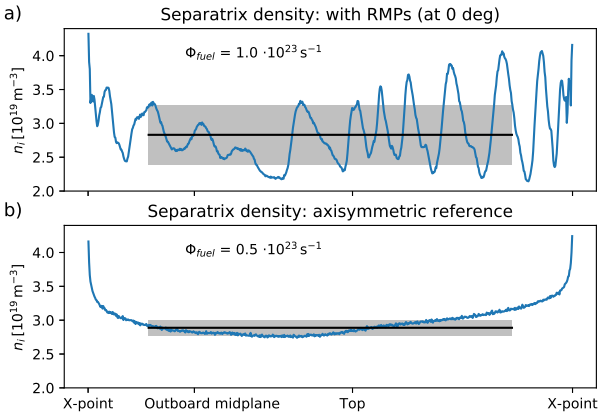

FIG. 4. Density profiles taken at the last radial cell index of the core zone (i.e. just inside the separatrix of the equilibrium configuration): (a) with RMPs, (b) axisymmetric reference without RMPs. The average value (black) and standard variation (gray) are taken after excluding 1/8 of the domain on either side of the X-point.

in figure 4 (a) taken just inside the equilibrium separatrix (evaluated at the last radial cell index of the core zone of the grid): the density varies quite significantly between $2.2 \cdot 10^{13}\,{\rm cm}^{-3}$ and $4.1 \cdot 10^{13}\,{\rm cm}^{-3}$. Without RMPs, on the other hand, the density remains largely flat except near the X-points, as can be seen in figure 4 (b). In the following we take the "flux surface averaged" $\overline{n}_{\rm up}$ (in toroidal and poloidal direction, but with 1/8 of the poloidal circumference excluded on either side of the X-point)[26] as characteristic parameter. Both simulations in figure 4 have comparable $\overline{n}_{\rm up} \approx 2.8 - 2.9 \cdot 10^{19}\,{\rm m}^{-3}$ despite requiring a factor 2 higher $\Phi_{\rm gas}$ when RMPs are present.

The helical oscillations of the perturbed separatrix bring field lines from the bulk plasma to the divertor targets. The resulting geometry is shown in figures 5 (a) and (b) for the inner and outer targets, respectively, where the radial connection $\mathcal{C}_r$ of field lines is represented by the minimum of the normalized poloidal flux ψ_N along a given field line. White and blue colors indicate scrape-off layer (SOL) -like field lines as known from the unperturbed configuration, and red colors indicate field lines connecting from the bulk plasma. The latter introduce a new type of exhaust channel with RMPs (that does not rely as much on cross-field transport through the separatrix and further into the SOL), and it can be seen in figure 5 (c-f) that it is those areas that dominate in terms of particle and heat loads. At this $\overline{n}_{\rm up}$, however, particle and heat loads are already reduced in the near SOL ($s \approx 0 - 10\,$cm) but not in the far SOL. This may be considered a partially detached state, but it should be noted that it is significantly different from a partially detached state of an axisymmetric configuration in that substantial particle and heat loads remain in the far SOL (see e.g. red profiles in figure 5 (c,d) and figure 2 (c) in

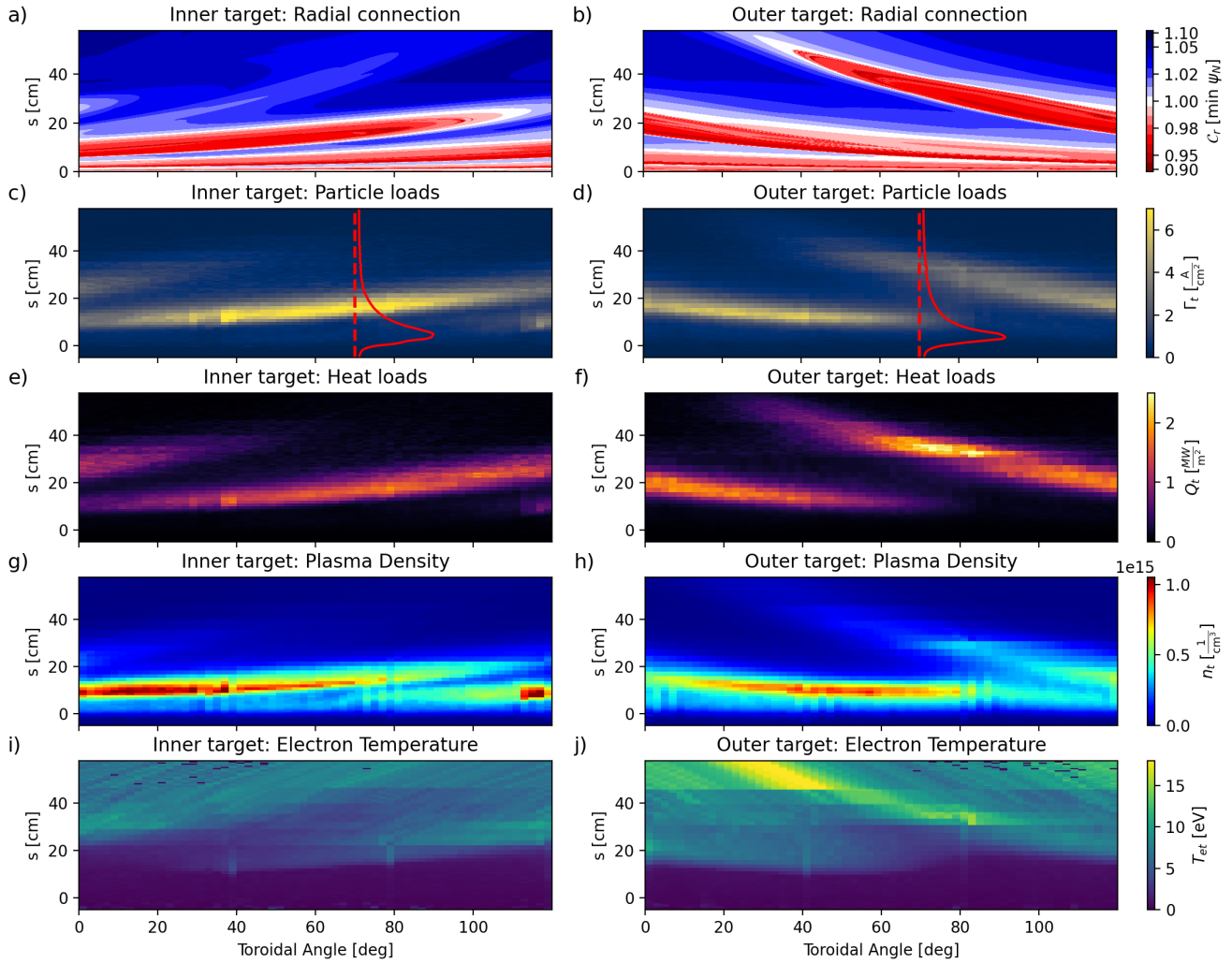

FIG. 5. Magnetic geometry and plasma parameters at the inner target (left column) and outer target (right column): (a,b) radial connection $\mathcal{C}_r$, (c,d) particle load Γ_t, (e,f) heat load Q_t, (g,h) plasma density n_t, and (i,j) electron temperature T_{et}. The shape of the unperturbed reference profiles are superimposed in (c,d) based on figure 6 (c-d).

reference 25). This is because of the direct field line connection from the bulk plasma (i.e. without the cross-field transport which would occur into the upstream far SOL in the axisymmetric configuration). Detachment at the traditional strike zone is consistent with the relatively high n_i and low T_e there, as can be seen in figure 5 (g-j).

For further evaluation of the divertor state, we integrate the local particle balance (2) along field lines from the target to the divertor entrance. For this we consider cross-field transport to be a source/sink on the field line

$$S_\perp = -\nabla \cdot \mathbf{\Gamma}_\perp, \qquad \mathbf{\Gamma}_\perp = -D_\perp \mathbf{e}_\perp \mathbf{e}_\perp \cdot \nabla n_i \tag{20}$$

so that the particle balance can be cast as an ordinary differential equation

$$|\mathbf{B}| \frac{d}{ds} \frac{\Gamma_\parallel}{|\mathbf{B}|} = S_p + S_{p\,vr} + S_\perp \tag{21}$$

for the particle flux $\Gamma_\parallel = n_i u_\parallel$ and after splitting off contributions from volumetric recombination from S_p. The left hand side follows from $\mathrm{div}\,\mathbf{B} = 0$ and introducing $\frac{d}{ds} = \mathbf{e}_\parallel \cdot \nabla$. Now we can link downstream (d) and upstream (u) locations on the same field line:

$$\Gamma_d = \underbrace{\frac{B_d}{B_u}\Gamma_u}_{=\Gamma_{dU}} + \underbrace{\int_u^d ds \frac{B_d}{|\mathbf{B}|}\left(S_p + S_{p\,vr} + S_\perp\right)}_{=\Gamma_{dN}+\Gamma_{d\,vr}+\Gamma_{d\perp}} \tag{22}$$

A post-processing tool has been implemented into EMC3-EIRENE which evaluates the upstream particle flux Γ_u and the integrals along magnetic field lines in (22) from simulation results [27]. For this, the cross-field transport term is approximated from

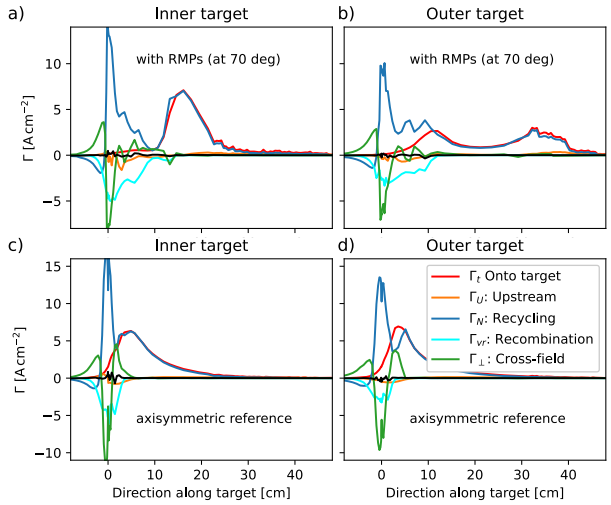

FIG. 6. Particle flux onto divertor targets with RMPs (upper row) evaluated at $\varphi = 70$ deg as indicated in figure 5 (c-d). This is compared to the reference case without RMPs (lower row). Contributions to Γ_t are resolved according to (24).

$$\overline{\nabla \cdot \mathbf{\Gamma}_\perp} = \frac{1}{V}\int_V dV\ \nabla \cdot \mathbf{\Gamma}_\perp = \frac{1}{V}\sum_{\text{radi, polo}} \Phi_{\perp\,\text{face}} \quad (23)$$

in each computational cell from the fluxes $\Phi_{\perp\,\text{face}}$ associated with cross-field transport across the cell boundaries (the "toroidal" grid direction is aligned with field lines and does not contribute here). The downstream flux contributions identified in (22) are then mapped onto the target surface along with Γ_d for an augmented analysis of the target load

$$\Gamma_t = \Gamma_U + \Gamma_N + \Gamma_{vr} + \Gamma_\perp \quad (24)$$

in terms of contributions from particles entering/leaving the divertor upstream (Γ_U), ionization of neutral particles in the divertor (Γ_N), recombination in the divertor volume (Γ_{vr}) and from cross-field transport ($\Gamma_\perp$). These contributions to Γ_t are evaluated in figure 6. It can be seen that a large number of recycled neutral particles (blue profiles) are lost through cross-field transport (green profiles) from the traditional strike zone (i.e. spread into the private flux region and further into the SOL) in both RMP and reference cases. This is supplemented by volumetric recombination (cyan profiles) which becomes the dominant sink for particles in the RMP case in the near SOL for $1.5\,\text{cm} \leq s \leq 10\,\text{cm}$. It has been highlighted in reference 25 that the onset of (partial) detachment occurs at lower upstream density due to reduced upstream heat flux with RMPs (evaluated in more detail in a separate study [28]), and this is supported here by the significantly broader reduction of Γ_t (red profiles) in the traditional SOL at comparable upstream densities with and without RMPs. The non-axisymmetric far SOL strike points, on the other hand, remain attached at relatively high T_e and low n_i, and neither cross-field transport nor volume recombination can act to reduce the particle load there from recycling neutral particles.

IV. DISCUSSION AND CONCLUSIONS

An upgrade to EMC3-EIRENE for detached divertor plasmas provides stabilization at low temperatures through linearization of the energy sink of the electron - neutral gas interactions. The implementation of an implicit method for volumetric electron - ion recombination has also been presented. Verification of the extended applicability range is indicated by good agreement with SOLPS-ITER results for the pre-fusion power operation phase in ITER for the same model parameters. A self-consistent particle balance in the plasma - neutral gas system has been verified down to the intrinsic noise level, and convergence acceleration by internal rescaling has been demonstrated. Dissipation from injected impurities has not been included here (because it is not necessary at relatively low heating power), but will be investigated in the future for the burning plasma operation phase where it is required.

A post-processing tool is included in the upgraded EMC3-EIRENE for an augmented analysis of divertor loads with spatially resolved contributions from ionization of neutral particles, recombination in the divertor volume, and from cross-field transport from and to adjacent field lines. Application of resonant magnetic perturbations for control of edge localized modes results in a partially detached divertor plasma with a significantly broader reduction of particle loads in the traditional strike zone than without RMPs, which is attributed to volumetric recombination. The additional non axisymmetric far scrape-off layer strike points, however, remain attached at relatively high temperature with significant particle and heat loads. This trade-off between near SOL and far SOL strike locations may initially be beneficial for minimizing divertor loads if it occurs at a moderate level, but can ultimately be more challenging if dissipation at the far SOL strike points cannot be achieved in burning plasmas.

Development and validation of plasma boundary models is an ongoing effort, and the present upgrade of EMC3-EIRENE is one step along the road. Yet to come are implementations of cross-field drifts and heat flux limits in EMC3, which remain the subject of further investigation. One particular challenge for 3-D plasma boundary models for RMPs is that a representation of the RMP field is required (in addition to the axisymmetric equilibrium field that is sufficient for 2-D models). We note that the results presented here depend considerably on the magnetic connection between bulk plasma and divertor targets, and plasma response effects play a pivotal

role for this. They have been included here based on MARS-F simulations, but this is only one of many different MHD models for plasma response to RMP application. Validation and benchmark of those models with a particular focus on the plasma boundary is required in order to allow reliable predictions for ITER, but this is far beyond the scope of this manuscript. For now, we content ourselves with taking a major step towards closing the gap in detachment physics between EMC3-EIRENE and state-of-the-art 2-D models, to be followed by cross-device benchmarks.

ACKNOWLEDGEMENTS

This work was supported by the U.S. Department of Energy under Awards No. DE-SC0020357, No. DE-SC0013911, and No. DE-SC0020284. This work was done under the auspices of the ITER Scientist Fellow Network. The views and opinions expressed herein do not necessarily reflect those of the ITER Organization.

DATA AVAILABILITY

The data that support the findings of this study are available from the corresponding author upon reasonable request.

Appendix A: Implementation of S_{ee} linearization

Implementation of this correction term requires evaluation of the temperature derivative of S_{ee}. Beside ionization ($e + D \rightarrow 2e + D^+$), several processes contribute to

$$S_{ee} = -n_e \cdot \sum_{P=D,D_2,D_2^+} n_P \cdot \sum_{e+P\rightarrow x} \langle \Delta E_x \, \sigma_x \, v \rangle \quad \text{(A1)}$$

were $\langle \Delta E_x \, \sigma_x \, v \rangle$ is the energy loss rate coefficient for the reaction $e + P \rightarrow x$. Double polynomial fits

$$\ln\langle \Delta \, \sigma \, v \rangle = \sum_{n=0}^{N} \sum_{m=0}^{M} \alpha_{n,m} \, (\ln n_e)^m \, (\ln T_e)^n \quad \text{(A2)}$$

are available from the AMJUEL and HYDHEL databases which supply EIRENE, and from this it is straightforward to evaluate the T_e-derivative (for given n_e). The new implementation of the coupling between EIRENE and EMC3 is based on the source decomposition form

$$S_{ee} = S_0 + T_e \cdot S_1 \quad \text{(A3)}$$

where S_1 accounts for the linearized T_e dependence of S_{ee}. Such a linearization can be stabilizing as long as $S_1 < 0$ [29], and we set

$$S_1^j = \min\left(0, \frac{dS_{ee}}{dT_e}\Big|_{T_e^{(j-1)}}\right) \quad \text{(A4)}$$

$$S_0^j = S_{ee}\left(T_e^{(j-1)}\right) - T_e^{(j-1)} \, S_1^j \quad \text{(A5)}$$

Energy loss rate coefficients increase with T_e, and so it follows from (A1) that $S_1^j < 0$ can indeed be achieved. Once S_0^j and S_1^j are passed to EMC3, the same explicit method as before is applied for the former. For the linearized term S_1^j, on the other hand, an implicit method is applied which is similar to that for volume recombination described in section II B in the main text.

[1] A. Kukushkin, H. Pacher, V. Kotov, G. Pacher, and D. Reiter, Finalizing the ITER divertor design: The key role of SOLPS modeling, Fusion Eng. Des. **86**, 2865 (2011).

[2] R. Pitts, X. Bonnin, F. Escourbiac, H. Frerichs, J. Gunn, T. Hirai, A. Kukushkin, E. Kaveeva, M. Miller, D. Moulton, V. Rozhansky, I. Senichenkov, E. Sytova, O. Schmitz, P. Stangeby, G. D. Temmerman, I. Veselova, and S. Wiesen, Physics basis for the first ITER tungsten divertor, Nuclear Materials and Energy **20**, 100696 (2019).

[3] S. Wiesen, D. Reiter, V. Kotov, M. Baelmans, W. Dekeyser, A. Kukushkin, S. Lisgo, R. Pitts, V. Rozhansky, G. Saibene, I. Veselova, and S. Voskoboynikov, The new SOLPS-ITER code package, J. Nucl. Mater. **463**, 480 (2015).

[4] X. Bonnin, W. Dekeyser, R. Pitts, D. Coster, S. Voskoboynikov, and S. Wiesen, Presentation of the New SOLPS-ITER Code Package for Tokamak Plasma Edge Modelling, Plasma Fusion Res. **11**, 1403102 (2016).

[5] T. E. Evans, R. A. Moyer, P. R. Thomas, J. G. Watkins, T. H. Osborne, J. A. Boedo, E. J. Doyle, M. E. Fenstermacher, K. H. Finken, R. J. Groebner, M. Groth, J. H. Harris, R. J. L. Haye, C. J. Lasnier, S. Masuzaki, N. Ohyabu, D. G. Pretty, T. L. Rhodes, H. Reimerdes, D. L. Rudakov, M. J. Schaffer, G. Wang, and L. Zeng, Suppression of Large Edge-Localized Modes in High-Confinement DIII-D Plasmas with a Stochastic Magnetic Boundary, Phys. Rev. Lett. **92**, 235003 (2004).

[6] A. Loarte, G. Huijsmans, S. Futatani, L. Baylor, T. Evans, D. M. Orlov, O. Schmitz, M. Becoulet, P. Cahyna, Y. Gribov, A. Kavin, A. S. Naik, D. Camp-

bell, T. Casper, E. Daly, H. Frerichs, A. Kischner, R. Laengner, S. Lisgo, R. Pitts, G. Saibene, and A. Wingen, Progress on the application of ELM control schemes to ITER scenarios from the non-active phase to DT operation, Nuclear Fusion **54**, 033007 (2014).

[7] Y. Feng, F. Sardei, and J. Kisslinger, 3D fluid modelling of the edge plasma by means of a Monte Carlo technique, Journal of Nuclear Materials **266-269**, 812 (1999).

[8] Y. Feng, H. Frerichs, M. Kobayashi, A. Bader, F. Effenberg, D. Harting, H. Hoelbe, J. Huang, G. Kawamura, J. D. Lore, T. Lunt, D. Reiter, O. Schmitz, and D. Sharma, Recent Improvements in the EMC3-Eirene Code, Contrib. Plasma Phys. **54**, 426 (2014).

[9] D. Reiter, M. Baelmans, and P. Boerner, The EIRENE and B2-EIRENE codes, Fusion Science and Technology **47**, 172 (2005).

[10] D. Reiter, EIRENE - A Monte Carlo linear transport solver, http://www.eirene.de.

[11] H. Frerichs, D. Reiter, Y. Feng, and D. Harting, Block-structured grids in Lagrangian 3D edge plasma transport simulations, Comp. Phys. Commun. **181**, 61 (2010).

[12] Y. Feng, H. Frerichs, M. Kobayashi, and D. Reiter, Monte-Carlo fluid approaches to detached plasmas in non-axisymmetric divertor configurations, Plasma Phys. Control. Fusion **59**, 034006 (2017).

[13] H. Frerichs and D. Reiter, Stability and control of iterated non-linear transport solvers for fusion edge plasmas, Comp. Phys. Commun. **188**, 82 (2015).

[14] H. Frerichs, X. Bonnin, Y. Feng, A. Loarte, R. Pitts, D. Reiter, and O. Schmitz, Stabilization of EMC3-EIRENE for detachment conditions and comparison to SOLPS-ITER, Nuclear Materials and Energy **18**, 62 (2019).

[15] ITER Organization, *ITER Research Plan within the Staged Approach*, Tech. Rep. ITR-18-003 (ITER Organization, 2018).

[16] V. Kotov, D. Reiter, R. A. Pitts, S. Jachmich, A. Huber, D. P. Coster, and J.-E. contributors, Numerical modelling of high density JET divertor plasma with the SOLPS4.2 (B2-EIRENE) code, Plasma Phys. Control. Fusion **50**, 105012 (2008).

[17] Y. Feng, F. Sardei, P. Grigull, K. McCormick, J. Kisslinger, D. Reiter, and Y. Igitkhanov, Transport in island divertors: physics, 3D modelling and comparison to first experiments on W7-AS*, Plasma Phys. Control. Fusion **44**, 611 (2002).

[18] It should be noted that even though temporal oscillations of the divertor state have been found [30, 31], the oscillations found here are intermediate states in an iterative approximation of a self-consistent steady state solution and are not necessarily related.

[19] The AMJUEL online database, http://www.eirene.de/html/amjuel.html.

[20] Note that H.10 includes the loss of thermal energy of the electrons, and that $S_{ee\,vr}$ is positive at low temperature and high densities.

[21] Y. Feng, J. Kisslinger, and F. Sardei, Formulation of a Monte Carlo model for edge plasma transport, in *27th EPS Conference on Contr. Fusion and Plasma Phys.*, Vol. 24B (Budapest, 2000) pp. 1188–1191.

[22] T. Lunt, H. Frerichs, M. Bernert, D. Brida, D. Carralero, M. Cavedon, P. David, A. Drenik, M. Faitsch, Y. Feng, M. Griener, A. Herrmann, B. Kurzan, O. Pan, U. Plank, D. Silvagni, M. Willensdorfer, M. Wischmeier, E. Wolfrum, and the ASDEX Upgrade team, Near- and far scrape-off layer transport studies in detached, small-ELM ASDEX Upgrade upper single-null discharges by means of EMC3-EIRENE, Plasma Phys. Control. Fusion **62**, 105016 (2020).

[23] Y. Q. Liu, A. Bondeson, C. M. Fransson, B. Lennartson, and C. Breitholtz, Feedback stabilization of nonaxisymmetric resistive wall modes in tokamaks. I. Electromagnetic model, Phys. Plasmas **7**, 3681 (2000).

[24] L. Li, Y. Q. Liu, A. Loarte, S. D. Pinches, A. Polevoi, Y. Liang, and F. C. Zhong, Modeling 3D plasma boundary corrugation and tailoring toroidal torque profiles with resonant magnetic perturbation fields in ITER, Nuclear Fusion **59**, 096038 (2019).

[25] H. Frerichs, O. Schmitz, X. Bonnin, A. Loarte, Y. Feng, L. Li, Y. Q. Liu, and D. Reiter, Detachment in Fusion Plasmas with Symmetry Breaking Magnetic Perturbation Fields, Phys. Rev. Lett. **125**, 155001 (2020).

[26] The average is taken toroidally and poloidally over cells at the last radial index. Even though the 3-D grid is constructed from (perturbed) field line tracing, the radial variation of the cell centers remains small within the grid domain: 1.2 ‰ of poloidal flux.

[27] Note that $S_{p\,vr}$ as introduced in (7) includes electron-ion recombination only. Even though processes leading to molecular assisted recombination (MAR) are included in the simulation, their contributions to $S_{p\,vr}$ are presently not explicitly resolved for technical reasons and remain implicitly included in S_p.

[28] H. Frerichs, X. Bonnin, Y. Feng, L. Li, Y. Q. Liu, A. Loarte, R. A. Pitts, D. Reiter, and O. Schmitz, Divertor detachment in the pre-fusion power operation phase in ITER during application of resonant magnetic perturbations, Nuclear Fusion **(submitted to)** (2021).

[29] S. V. Patankar, *Numerical Heat Transfer and Fluid Flow*, edited by W. J. Minkowycz and E. M. Sparrow (McGraw-Hill Inc.,US, 1980).

[30] S. I. Krasheninnikov, A. S. Kukushkin, and A. A. Pshenov, Divertor plasma detachment, Phys. Plasmas **23**, 055602 (2016).

[31] R. D. Smirnov, A. S. Kukushkin, S. I. Krasheninnikov, A. Y. Pigarov, and T. D. Rognlien, Impurity-induced divertor plasma oscillations, Phys. Plasmas **23**, 012503 (2016).